THE JOURNAL OF BIOLOGICAL CHEMISTRY
Vol. 280, No. 2, Issue of January 14, pp. 1661–1668, 2005
Printed in U.S.A.

Structural Dissection of a Highly Knotted Peptide Reveals Minimal Motif with Antimicrobial Activity*[S]

Received for publication, September 14, 2004, and in revised form, October 15, 2004
Published, JBC Papers in Press, October 19, 2004, DOI 10.1074/jbc.M410577200

Miquel Vila-Perelló‡§, Andrea Sánchez-Vallet¶, Francisco García-Olmedo¶, Antonio Molina¶, and David Andreu‡‖

From the ‡Department of Experimental and Health Sciences, Pompeu Fabra University, Dr. Aiguader, 80, E-08003 Barcelona, Spain and the ¶Biochemistry Laboratory, Biotechnology Department, UPM-ETSIA, Avda. Complutense, E-28040 Madrid, Spain

The increasing occurrence of bacterial resistance to antibiotics is driving a renewed interest on antimicrobial peptides, in the hope that understanding the structural features responsible for their activity will provide leads into new anti-infective drug candidates. Most chemical studies in this field have focused on linear peptides of various eukaryotic origins, rather than on structures with complex folding patterns found also in nature. We have undertaken the structural dissection of a highly knotted, cysteine-rich plant thionin, with the aim of defining a minimal, synthetically accessible, structure that preserves the bioactive properties of the parent peptide. Using efficient strategies for directed disulfide bond formation, we have prepared a substantially simplified (45% size reduction) version with undiminished antimicrobial activity against a representative panel of pathogens. Analysis by circular dichroism shows that the downsized peptide preserves the central double α-helix of the parent form as an essential bioactive motif. Membrane permeability and surface plasmon resonance studies confirm that the mechanism of action remains unchanged.

Antimicrobial peptides (1–4) are important constituents of the innate immune system (5) of most organisms and have been postulated as one of the most ancient weapons devised by evolution to fight bacterial infections (3). Their swift mobilization in the early stages of microbial invasion fulfills a crucial role in host defense, before the onset of cell-mediated immune response, which occurs slowly compared with microbial proliferation (6, 7). The increasingly high number of bacteria that are developing resistance to classical antibiotics (8–10) drives much of the current interest on antimicrobial peptides, in the hope that understanding the structural features responsible for the activity of these natural products (11–14) may provide useful leads into new anti-infective drug candidates. Such expectations are sustained on the relatively simple mechanism of action of antimicrobial peptides that, in contrast to classical antibiotics, involves simple disruption of microbial plasma membranes rather than complex intracellular targets and pathways. For pathogens to develop resistance to membrane-acting peptides, substantial membrane redesign would be required, a non-affordable solution for most species.

Following earlier studies on linear antimicrobial peptides (15, 16), we have recently focused our attention on plant thionins (17), the first family of antimicrobial peptides for which *in vitro* activity against plant pathogens (18) and a defensive role (19) were reported. Despite their early discovery, the potential of thionins and other plant antibiotic peptides (20) in medicine remains almost unexplored because most work on membrane active peptides has focused, until recently (21) on peptide families isolated from mammals, amphibians or insects (bbcm.univ.trieste.it/~tossi/pag1.htm contains a complete collection of gene-encoded antimicrobial peptides). Thionins are basic, 45–47-residue long, highly folded, disulfide-rich peptides classified into five structural types on the basis of amino acid sequence and cysteine pairing (22). Despite some inter-species diversity, all thionins share an almost identical folding pattern consisting of a short β-sheet and a pair of antiparallel α-helices connected through a β-turn (Fig. 1). Disulfide bonds play a crucial role in stabilizing thionin folding, providing a characteristic amphipathic distribution of residues that is thought to be responsible for their ability to strongly interact and disrupt microbial and model membranes (23).

There have been some attempts to decipher generally conserved structural motifs on antimicrobial peptides (26). We describe here our search for a minimal active structure for the thionin from *Pyrularia pubera* (PpTH),[1] a highly knotted peptide representative of this cysteine-stabilized family of membrane-active peptides. Our dissection of the native PpTH structure has led to several shortened versions, and eventually shown that the central antiparallel double helix of PpTH is fully active against representative plant pathogens. We have used surface plasmon resonance (SPR) to show that the affinity of this mini-thionin for artificial membranes is comparable with that of the native peptide, and demonstrated that the ability to bind model membranes correlates with antimicrobial activity. Experiments with the SYTOX Green dye have shown that all active peptides permeabilize in a similar way the

* This work was supported in part by Spanish Ministry of Science and Technology Grants BIO2002-04091-C03-01 and BIO2000-1308 (to D. A. and A. M., respectively). The costs of publication of this article were defrayed in part by the payment of page charges. This article must therefore be hereby marked "*advertisement*" in accordance with 18 U.S.C. Section 1734 solely to indicate this fact.

[S] The on-line version of this article (available at http://www.jbc.org) contains additional text.

§ Supported by a Department of Universities and Research of Generalitat de Catalunya, Spain, predoctoral fellowship.

‖ To whom correspondence should be addressed: Dept. of Experimental and Health Sciences, Pompeu Fabra University, Dr. Aiguader 80, 08003 Barcelona, Spain. Tel.: 34-935422934; Fax: 34-935422802; E-mail: david.andreu@upf.edu.

[1] The abbreviations used are: PpTH, *Pyrularia pubera* thionin; SPR, surface plasmon resonance; Rink amide linker, 2,4-dimethoxy-4′-(carboxymethyloxy)-benzhydrylamine; Fmoc, 9-fluorenylmethoxycarbonyl; Acm, acetamidomethyl; DMPC, 1,2-dimyristoyl-*sn*-glycero-3-phosphocholine; DMPG, 1,2-dimyristoyl-*sn*-glycero-3-phospho-*rac*-(1-glycerol); HPLC, high performance liquid chromatography; MALDI-TOF MS, matrix-assisted laser desorption ionization time-of-flight mass spectrometry.

plasma membrane of the fungal plant pathogen *Fusarium oxysporum*. We also show that a well defined secondary structure, prior to membrane binding, is required for the peptide to display any relevant antimicrobial activity. Our results are discussed in the light of recent advances in the understanding of the mechanism of action of antimicrobial peptides.

EXPERIMENTAL PROCEDURES

Materials

Fmoc-protected amino acids were purchased from Senn Chemicals (Dielsdorf, Switzerland). Polyethylene glycol-polystyrene resin was from Applied Biosystems (Foster City, CA). *p*-Methylbenzhydrylamine resin and the 2,4-dimethoxy-4′-(carboxymethyloxy)-benzhydrylamine (Rink amide) linker were from Bachem (Bubendorf, Switzerland). 2-(1*H*-Benzotriazol-1-yl)-1,1,3,3-tetramethyluronium hexafluorophosphate and *N*-hydroxybenzotriazole were from Albatross Chemicals (Montreal, Canada). HPLC-grade acetonitrile, peptide synthesis-grade *N*,*N*-dimethylformamide and trifluoroacetic acid were from SDS (Peypin, France). Other reagents were from Sigma.

Bacterial pathogens *Clavibacter michiganensis* subsp. *sepedonicus*, strain C5, *Xanthomonas campestris* pv. *campestris*, and *Rizhobium meliloti* were from the ETSIA collection (Madrid, Spain), and the fungal plant pathogen *F. oxysporum* f. sp. *conglutinans*, was a gift of Dr. M. L. G. Roncero (Cordoba University, Spain). Nutrient broth was from Oxoid (Basingstoke, UK) and potato dextrose from Difco (Detroit, MI).

Chromatography and Mass Spectrometry

Analytical reversed-phase HPLC was done on a Shimadzu LC-2010A system using a Phenomenex Luna C8 column (3 μm, 0.46 $\times$ 5 cm). Separations were performed using a linear gradient (10–40%) of buffer B into buffer A over 15 min at a flow rate of 1 ml/min. Buffer A was 0.045% trifluoroacetic acid in water. Buffer B was 0.036% trifluoroacetic acid in acetonitrile. Preparative HPLC runs were performed on a Shimadzu LC-8A instrument using a Phenomenex Luna C8 column (10 μm, 2.1 $\times$ 25 cm) eluted with the above gradient over 60 min at a flow rate of 25 ml/min. Mass spectrometric analysis of peptides was performed on a Voyager DE-STR instrument (Applied Biosystems, Foster City, CA) using α-cyano-4′-hydroxycinnamic acid as matrix.

Peptide Synthesis

Four-disulfide Peptides—PpTH-(3–41) and PpTHR-(3–41) (Table I), with native-like folding pattern, were prepared as C-terminal carboxamides from a linear octathiol precursor assembled by Fmoc solid phase synthesis protocols (27) on Rink amide-polyethylene glycol-polystyrene at 0.1-mmol scale in an Applied Biosystems 433A instrument. Side chain protections were *tert*-butyloxycarbonyl (Lys, Trp), *tert*-butyl (Ser, Asp, Glu), trityl (Asn, Cys), and 2,2,4,6,7-pentamethyldihydrobenzofuran-5-sulfonyl (Arg). Couplings were performed with 10 eq (1 mmol) each of Fmoc-amino acid 2-(1*H*-benzotriazol-1-yl)-1,1,3,3-tetramethyluronium hexafluorophosphate and *N*-hydroxybenzotriazole, in the presence of 20 eq of *N*,*N*-diisopropylethylamine in *N*,*N*-dimethylformamide. Total deprotection and cleavage from the solid support were done with trifluoroacetic acid/thioanisole/water/phenol/ethanedithiol (82.5:5:5:5:2.5) for 3.5 h at room temperature. Peptides were isolated by precipitation with cold *tert*-butyl methyl ether and centrifugation, then taken up in 10% acetic acid and lyophilized. The crude product was purified by preparative HPLC. Fractions containing >95% (by analytical HPLC) of the expected octathiol (by MALDI-TOF MS) were pooled, dissolved (argon atmosphere) to 5 μM in 0.1 M ammonium acetate, pH 7.8, and oxidatively folded as described (17) in the presence of 1 M guanidinium chloride and reduced and oxidized glutathione (1:100:10 molar ratio of peptide:GSH:GSSG). After 8 h at 25 °C the major HPLC product gave a negative Ellman test upon which the reaction was quenched with trifluoroacetic acid (to pH 2) and the mixture purified by preparative HPLC and characterized as above.

Two-disulfide Peptides—PpTH-(7–32) and PpTHR-(7–32) (Table I), two 26-residue analogues, were prepared by stepwise disulfide formation (28) from linear precursors assembled by Fmoc solid phase methods on Rink amide-*p*-methylbenzhydrylamine resin as above, except that Cys residues (6 and 25) corresponding to positions 12 and 31 of the native sequence were protected with the acetamidomethyl (Acm) group. Deprotection and cleavage from the resin with trifluoroacetic acid/triisopropylsilane/water/phenol/EDT (82.5:5:5:5:2.5, 2 h at room temperature) gave partially protected ($Cys^{6,25}$(Acm)) derivatives that, after preparative HPLC purification, were dissolved at 15 μM concentration in 0.1 M Tris, pH 8.0, and stirred under air until oxidation was shown to be complete by both the Ellman test and MALDI-TOF MS analysis of the major HPLC peak. The solution was then made up to 15% acetic acid and the Acm groups were removed simultaneously with Cys oxidation by dropwise addition of 4 eq of iodine (freshly prepared 5 mM solution in methanol). HPLC analysis showed the oxidation to be complete after 10 min. The reaction mixture was treated with sodium thiosulfate to stop the oxidation and directly loaded onto a preparative HPLC column. Fractions containing >95% (by analytical HPLC) of the expected double disulfide products were pooled and further characterized by amino acid analysis and MALDI-TOF MS.

Single Disulfide and Linear Peptides—PpTH-(24–32), PpTHR-(24–32), PpTH-(15–28), and PpTH-(7–19) (Table I) were assembled in a Syro multiple synthesizer (MultiSyntech, Witten, Germany) by Fmoc solid phase methods on Rink amide-*p*-methylbenzhydrylamine resin as above. PpTH-(15–28) peptide containing a Cys pair was deprotected with trifluoroacetic acid/water/triisopropylsilane/EDT (92.5:2.5:2.5:2.5, 2 h at room temperature), whereas for linear peptides trifluoroacetic acid/water/triisopropylsilane (95:2.5:2.5, 2 h at room temperature) was

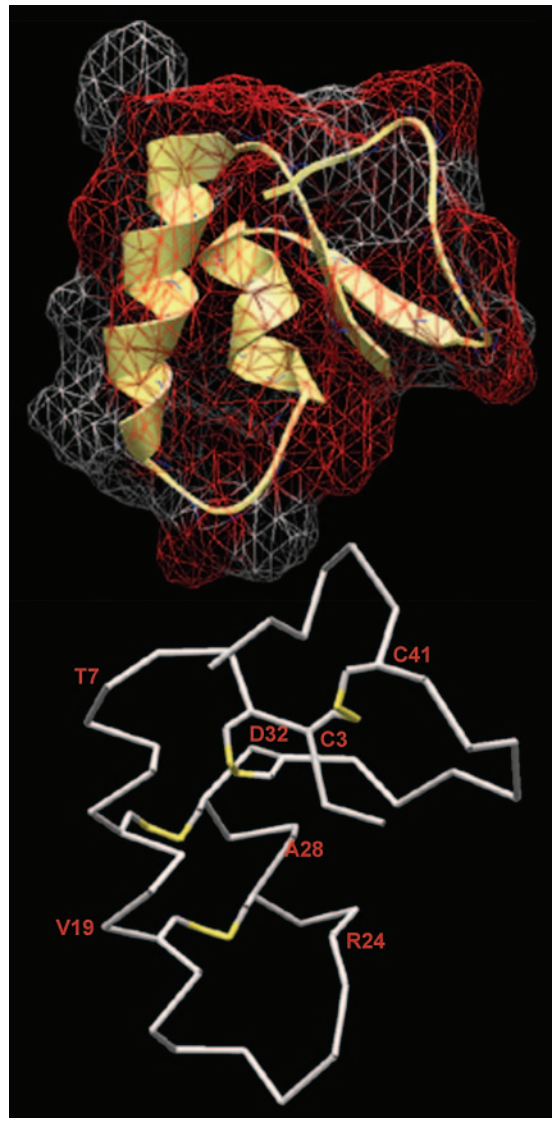

FIG. 1. **Three-dimensional structure of *P. pubera* thionin.** *Top panel*, PpTH displays the typical three-dimensional structure of the thionin family, resembling the Greek capital letter gamma (Γ). Hydrophilic residues (in *red*) cluster at the inner surface of the long arm of the Γ and at the region above its short arm, whereas hydrophobic residues (*light gray*) mainly occur on the outer face of the long arm of the Γ. *Bottom panel*, α-carbon trace of PpTH with the residues chosen as boundaries for thionin dissection labeled in *red*. The structure was calculated by homology modeling with the SWISS-MODEL server and further refined by molecular dynamics simulations with the MOLARIS (24) package. Molecular surface was calculated using Swiss PDB Viewer 3.7 software (25).

TABLE I
Sequences and molecular weight of all synthesized peptides

Name	Sequence	MW_{obs}	MW_{calc}
PpTH	KSCCRNTWARNCYNVCRLPGTISREICAKKCDCKIISGTTCPSDYPK	5380.28	5380.17[a]
PpTH(3-41)	CCRNTWARNCYNVCRLPGTISREICAKKCDCKIISGTTC	4375.93	4376.19[a]
PpTHR(3-41)	CCRNTWARNCYNVCRLPGTISREICAKKCRCKIISGTTC	4417.83	4417.29[a]
PpTHR(7-32)	TWARNCYNVCRLPGTISREICAKKCR	3037.41	3037.61[a]
PpTH(7-32)	TWARNCYNVCRLPGTISREICAKKCD	2994.40	2994.42[b]
PpTH(7-32)b	TWARNCYNVCRLPGTISREICAKKCD	2994.39	2994.42[b]
PpTH(24-32)	REISAKKSD	1031.46	1031.57[b]
PpTHR(24-32)	REISAKKSR	1072.70	1072.65[b]
PpTH(7-19)	TWARNSYNVSRLP	1562.75	1562.80[b]
PpTH(15-28)	VCRLPGTISREICA	1514.61	1514.77[b]

[a] Average molecular weight.
[b] Monoisotopic molecular weight.

used. The dithiol precursor of PpTH-(15–28) was air-oxidized at 10 μM concentration in 0.1 M ammonium bicarbonate, pH 8.1, for 24 h. Oxidation was quenched by trifluoroacetic acid addition to pH 1.5–2. All peptides were purified by preparative HPLC to give products with amino acid analyses and MS consistent with theory.

Circular Dichroism

CD spectra in the 190–260-nm range were acquired on a Jasco J715 spectropolarimeter purged with nitrogen (25 ml/min) and using a quartz 0.1-cm path length cell stabilized to ±0.1 °C of the desired temperature by a Peltier controller. Spectra of all peptides were recordered at 15 μM concentration in 25 mM phosphate, pH 6.0, in the absence and presence of small unilamellar vesicles of dimyristoyl phosphatidylglycerol (DMPG) at a peptide/lipid ratio of 1:100. Small unilamellar vesicles were prepared by dissolving dry DMPG in chloroform/methanol (2:1), removing the solvents in a rotary evaporator, and hydrating the residue (to 3 mM DMPG concentration) in 25 mM phosphate, pH 6.0, for 1 h at room temperature. The suspension was first mixed in a vortex shaker, then sonicated until clear.

Antimicrobial Activity

The antimicrobial tests were done in sterile 96-well microplates by mixing different amounts of the peptides dissolved in 66.7 μl of sterile water with 33.3 μl of bacterial suspension (final concentration 10^4 colony forming units/ml) in nutrient broth or TY medium (*R. meliloti* (29)), or 33.3 μl of *F. oxsyporum* spore suspension (final concentration, 10^4 spores/ml) in potato dextrose. Microorganisms were incubated at 28 °C with periodic agitation and growth was recorded 24–48 h later by measuring absorbance at 490 nm in an enzyme-linked immunosorbent assay plate reader.

SYTOX Permeation Experiments

For SYTOX green uptake different amounts of the peptides dissolved in 25 μl of sterile water were mixed with 12.5 μl of *F. oxsyporum* spore suspension (final concentration 2×10^4 spores/ml) in potato dextrose, the microplate was incubated at 28 °C for 6 h, and 0.75 μl of SYTOX Green (0.2 μM final concentration) was added to the wells. After 18 h of additional incubation fungal hyphae fluorescence was viewed with a microscope (Zeiss AxioPhot, Germany) equipped with a B-2A filter set for fluorescence detection (excitation wavelength, 450–490 nm; emission wavelength, 520 nm). Light and fluorescence microscopic images were taken with a video camera (SPOT33, Diagnostic Instrument Inc.) and analyzed using the SPOT33 2.2 software.

Surface Plasmon Resonance

Measurements were carried out on a BIAcore 3000 instrument (Biacore, Uppsala, Sweden) using a L1 sensor chip with a carboxymethylated dextran matrix modified with lipophilic units to capture lipid bilayer vesicles. Phosphate-buffered saline, pH 6.8, was used as run-

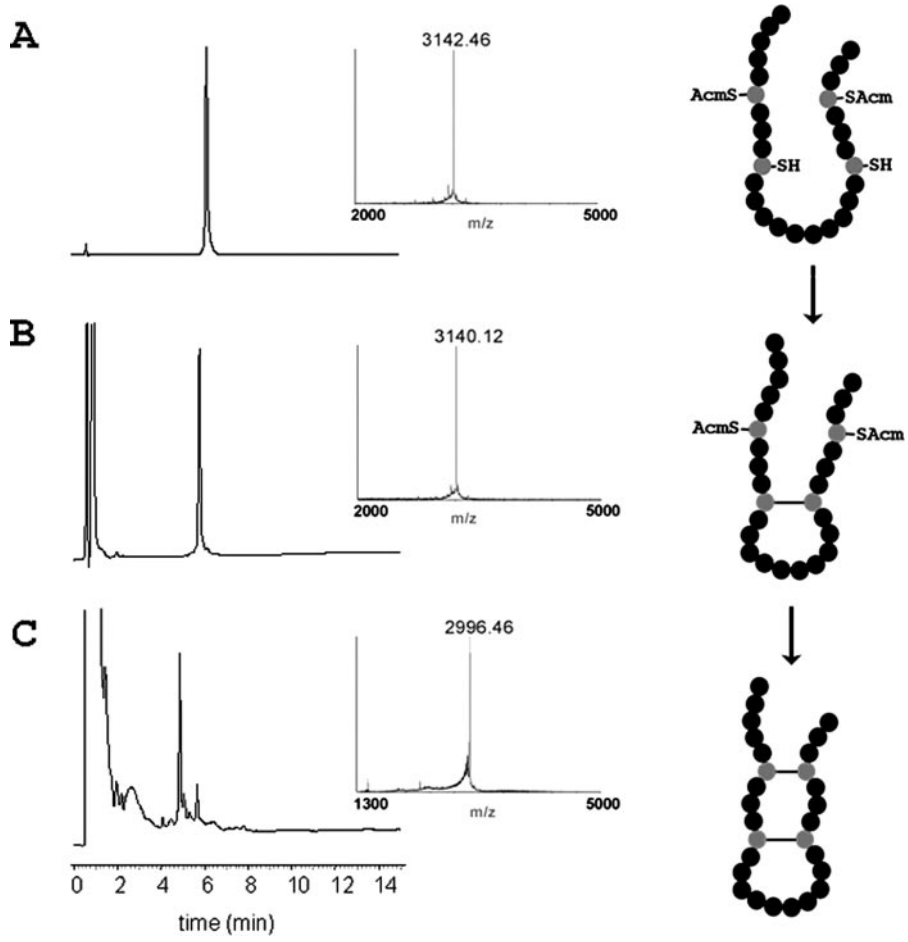

FIG. 2. **Synthetic route to PpTH-(7–32) and PpTHR-(7–32) by a two-step chemoselective disulfide bond formation strategy.** *A*, HPLC profile and MALDI-TOF MS of purified and totally reduced PpTH-(7–32) with two Acm protecting groups. *B*, formation of the first disulfide bond by air oxidation of deprotected Cys residues: HPLC analysis of the oxidation crude after a 20-h reaction and MALDI-TOF MS of the major peak. *C*, formation of the second disulfide bond by iodine-promoted simultaneous deprotection-oxidation of Cys^{6}-Cys^{25}: HPLC profile of the crude reaction mixture and MALDI-TOF MS analysis of the main peak.

ning buffer and regeneration and washing solutions were 10 mM NaOH and 40 mM *N*-octyl-β-glucopyranoside, respectively. All solutions were freshly made, degassed, and filtered through a 0.22-μm filter. Large unilamellar vesicles (100 nm) with a 3:1 DMPC/DMPG ratio were prepared by dissolving the dry lipids in chloroform/methanol (2:1). After solvent removal by rotary evaporation, the lipids were suspended in phosphate-buffered saline, pH 6.8, by sonication, and liposomes of the desired size were obtained by sequentially extruding the resultant emulsion through 0.8-, 0.4-, 0.2-, and 0.1-μm filters (5 passages through each filter). Prior to immobilization of the DMPC/DMPG large unilamellar vesicles on the L1 chip, an injection of 25 μl of 40 mM *N*-octyl-β-glucopyranoside at 5 μl/min flow rate was performed to clean the surface. Liposomes were applied to the sensor surface at a flow rate of 2 μl/min. Between each liposome injection, a 10 mM NaOH pulse was applied to remove multilamellar structures. Once the desired immobilization level (above 5000 response units) was reached, the active surface was stabilized by repeated injections of 10 mM NaOH and buffer until a stable baseline was obtained. Further details are provided as Supplementary Materials.

Peptides were dissolved in phosphate-buffered saline at concentrations in the 5–100 μM range and injected (40 μl) at 10 μl/min flow rate on the liposome-loaded sensor chip. Peptide solution was next replaced by running buffer and the peptide-bilayer complex was allowed to dissociate for 5 min. Because peptides bind very tightly to the liposomes, no complete regeneration of the active surface was possible in this way and full removal of the immobilized bilayer had to be achieved by pulsing with 10 mM NaOH and 10 mM HCl (50 μl each) followed by a 30-μl wash with 40 mM *N*-octyl-β-glucopyranoside at 5 μl/min flow rate.

Sensorgrams for each peptide-lipid interaction were analyzed by curve fitting using numerical integration algorithms in the BIAevaluation 3.0 software package. Recorded sensorgrams at seven different concentrations were globally fitted using a two-state binding model, as poorer fitting was obtained using simpler models (*e.g.* 1:1 Langmuir binding). Equations used in the fitting process are detailed under Supplementary Materials.

RESULTS

Peptide Design and Synthesis—To elucidate which structural motifs are responsible for the antimicrobial activity of PpTH (Fig. 1), several peptides reproducing different regions were designed (Table I). PpTH-(3–41) is a shortened version of PpTH, with both N- and C-terminal deletions but preserving the four disulfide arrangement. PpTHR-(3–41) is a PpTH-(3–41) analogue where the Asp^{32} residue is mutated to Arg, a modification shown to significantly enhance the antimicrobial activity of full-length PpTH against Gram-negative bacteria (17). Other peptides were meant to reproduce secondary structure elements such as each one of the helical segments (PpTH-(7–19) and PpTH-(24–32)), the intervening loop (PpTH (15–28)), or the double antiparallel α-helix motif (PpTH-(7–32)), which given its amphipathic character, might be a key feature for antimicrobial activity. For all analogues containing the Asp residue at position 32 of the native sequence, the corresponding Arg replacement analogue was also synthesized to explore whether the positive effect of this mutation was maintained throughout the series. Disulfide pairings corresponding to native PpTH were preserved in all peptides except PpTH-(7–32)b, where the alternative connectivity was explored to evaluate the importance of disulfide bridges for the secondary structure and activity of this particular structure.

For the four-disulfide peptides, PpTH-(3–41) and PpTHR-(3–41), synthesis and folding protocols previously developed for full-length thionins (17) were successfully adapted. The oxidation reaction was remarkably clean, allowing for combined folding-purification yields in the 30% range. The folded peptides had the expected amino acid compositions and molecular masses 8.0 Da less than their octathiol precursors (Table I).

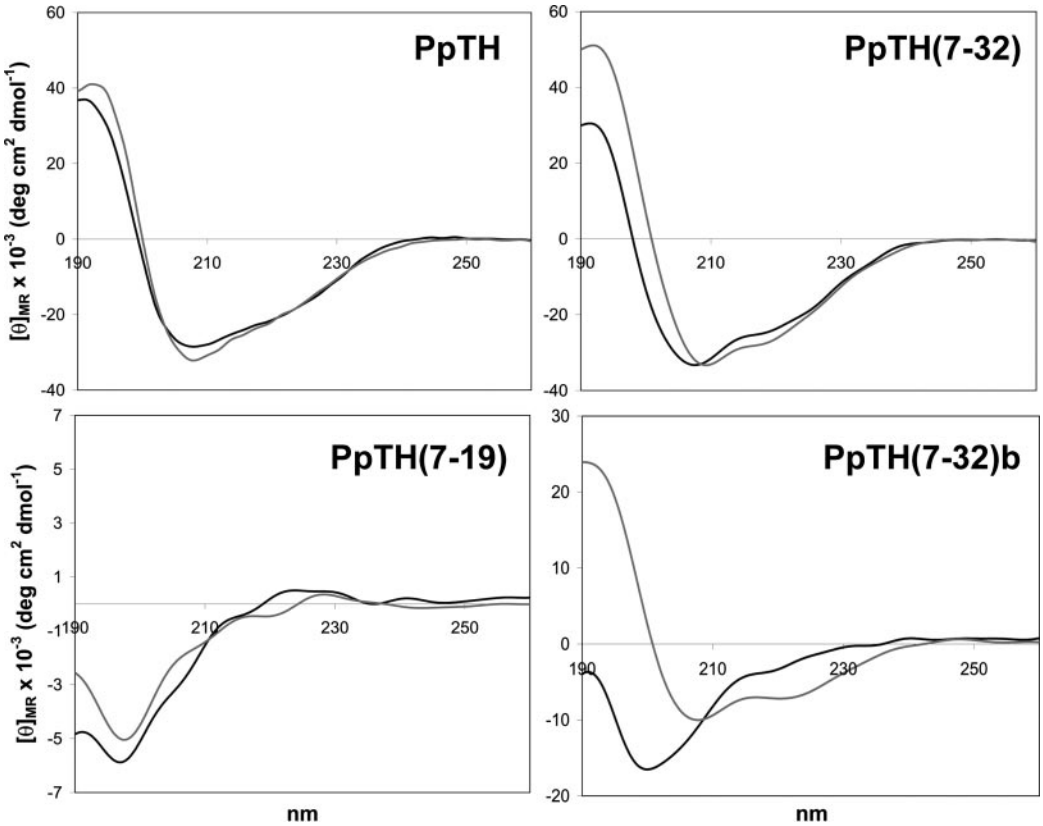

FIG. 3. **Conformational changes of thionin analogues upon binding to model membranes.** CD curves of PpTH, PpTH-(7–32), PpTH-(7–19), and PpTH-(7–32)b at 15 μM at 5 °C; peptides in 25 mM phosphate buffer, pH 6.0 (*black lines*) and in the presence of DMPG small unilamellar vesicles (*gray lines*) are shown.

Attempts to synthesize the double-disulfide PpTH-(7–32) by a similar oxidative folding procedure led to a mixture where a misfolded analogue, PpTH-(7–32)b (see Table I), predominated over the expected product. PpTH-(7–32) was more efficiently accessible by a two-step strategy of directed disulfide formation (28, 30) where Cys^6 and Cys^{25} and Cys^{10} and Cys^{21} were, respectively, protected with the Acm and trityl groups (Fig. 2). The Cys^{10}-Cys^{21} disulfide bridge was generated practically quantitatively by air oxidation at pH 8.0 and followed by iodolytic removal of the two Acm groups and concomitant formation of the second disulfide bond under mild conditions at room temperature. An entirely analogous approach was used to prepare the Arg replacement analogue PpTHR-(7–32). Following preparative HPLC purification, both peptides and the misfolded PpTH-(7–32)b analogue were satisfactorily characterized by amino acid analysis and MS (Table I), and their disulfide connectivity corroborated by tryptic digestion of the folded peptides and MS analysis of the fragments (see Supplementary Materials). The remaining peptides (single disulfide PpTH-(15–28), and linear PpTH-(7–19) and PpTH-(24–32)) were prepared by standard Fmoc solid phase synthesis methods (27).

Circular Dichroism—CD spectra of PpTH-(3–41), PpTH-(7–32) and their Arg^{32} analogues PpTHR-(3–41) and PpTHR-(7–32) in aqueous solution were almost identical to those of native PpTH and consistent with a mainly α-helical structure coexisting with some levels of β-type structure. Upon binding to anionic DMPG liposomes, the global pattern of CD signatures was maintained, with slight decreases in helical content for the larger PpTH-(3–41) and PpTHR-(3–41) peptides, whereas the smaller PpTH-(7–32) and PpTHR-(7–32) reinforced their helical character (Fig. 3, Table II). Temperature studies for these four peptides in the 5–85 °C range showed the helical pattern mostly preserved throughout the interval, as for native thionin (17) (see Supplementary Materials). At elevated temperatures slight decreases in helical content were detected; globally, the temperature dependence pattern of molar ellipticity at 207 nm fitted with a non-cooperative thermal unfolding pathway.

TABLE II
α-Helical percentage, in buffer and in the presence of SUV, of all studied PpTH peptides

	α-Helix[a]	
	In buffer[b]	Bound to SUV[c]
PpTH	53.3	53.3
PpTH-(3–41)	43.9	37
PpTHR-(3–41)	49.6	40.5
PpTH-(7–32)	65.4	68.3
PpTH-(7–32)b	RC[d]	19.9
PpTHR-(7–32)	68.2	78.8
PpTH-(7–19)	RC	RC
PpTH-(24–32)	RC	RC
PpTHR-(24–32)	RC	RC
PpTH-(15–28)	RC	17.6

[a] % α-Helix estimated by the Yang equations (31, 32).
[b] 15 μM peptide, 25 mM phosphate buffer, pH 6.0.
[c] 15 μM peptide in the presence of DMPG liposomes (1:100 peptide/lipid ratio), 25 mM phosphate buffer, pH 6.0.
[d] RC, ramdom coil conformation.

The spectra of shorter PpTH-(7–19) and PpTH-(24–32), reproducing each of the helical fragments of PpTH, were typical of aperiodic structure and unaffected by liposomes. Interestingly, PpTH-(15–28) and PpTH-(7–32)b peptides exhibited an intermediate behavior, with no preferred conformation in aqueous solution but adopting a certain level (about 20%) of helicity on binding to negatively charged liposomes.

Antimicrobial and Permeabilizing Activity—In vitro activities of the synthetic peptides against one Gram-positive and two Gram-negative bacteria, and a fungal plant pathogen are

TABLE III
Inhibition of bacterial and fungal plant pathogen growth by PpTH peptides

Peptide[b]	EC_{50} (μM)[a]			
	Gram positive *C. michiganensis*	Gram negative		Fungi *F. oxysporum*
		R. meliloti	*X. campestris*	
PpTH	0.23 ± 0.04	>20 ± 0	3.67 ± 0.58	0.38 ± 0.08
PpTHR	0.23 ± 0.0	3.8 ± 0	0.38 ± 0.04	1.52 ± 0.79
PpTH-(3–41)	0.18 ± 0.05	>20 ± 0	7.5 ± 0.5	1.73 ± 0.21
PpTHR-(3–41)	0.21 ± 0.11	5.3 ± 0	3.27 ± 0.64	2.5 ± 0
PpTH-(7–32)	0.63 ± 0.13	>20 ± 0	>20 ± 0	1.80 ± 0
PpTHR-(7–32)	1.58 ± 0.28	4 ± 0	7.2 ± 0	0.5 ± 0
PpTH-(7–32)b	1.8 ± 0	>20 ± 0	>20 ± 0	>20 ± 0
PpTH-(24–32)	>20 ± 0	>20 ± 0	>20 ± 0	>20 ± 0
PpTHR-(24–32)	16 ± 5.6	>20 ± 0	>20 ± 0	>20 ± 0
PpTH-(15–28)	>20 ± 0	>20 ± 0	>20 ± 0	>20 ± 0
PpTH-(7–19)	15 ± 2.5	>20 ± 0	>20 ± 0	>20 ± 0

[a] Effective concentration for 50% inhibition (mean of three experiments ± S.D.).
[b] Named according to Table I.

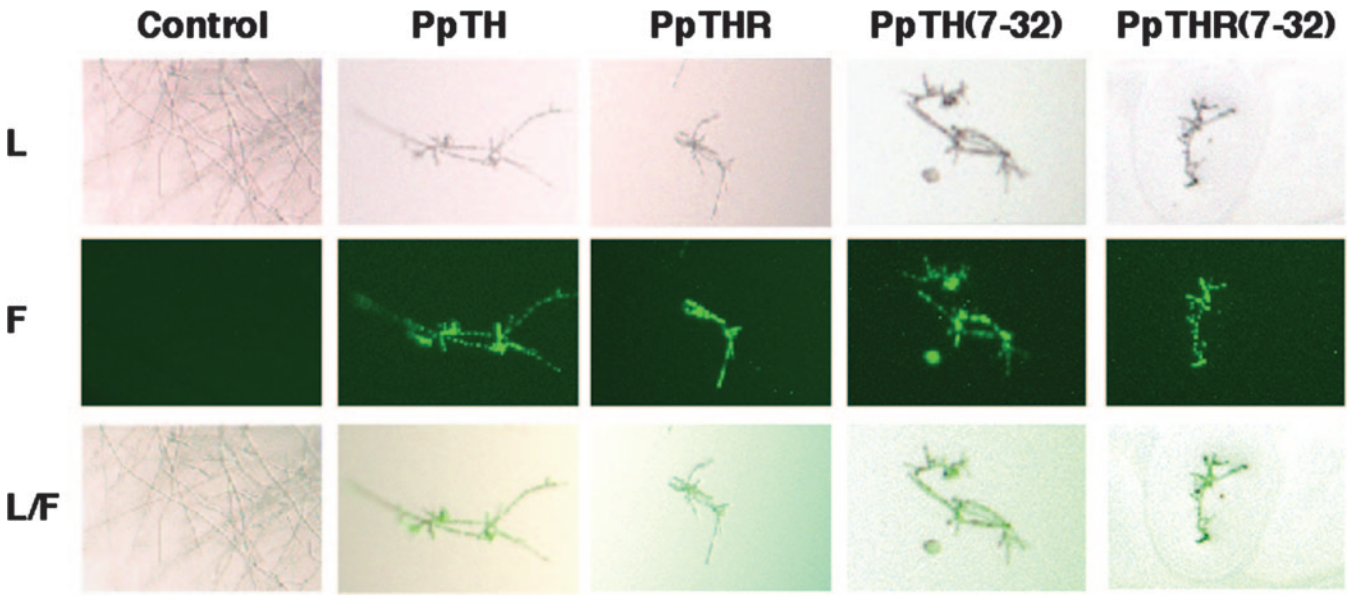

FIG. 4. **Membrane permeation studies by influx of SYTOX dye into fungal hyphae.** Fluorescence microscopy of *F. oxysporum* hyphae incubated with 0.2 μM SYTOX Green in the absence (control) or with 2-fold EC_{50} concentrations of the indicated PpTH peptides. Dye penetration by the effect of all active peptides is clearly observed. *Upper panels*, light microscopy (*L*); *middle panels*, fluorescence images (*F*); *lower panels*, superimposition of both L and F images (*L/F*).

shown in Table III. As previously described (17) PpTHR was significantly more active than PpTH against the Gram-negative bacteria, whereas activity against the Gram-positive organism and the fungus were comparable. The shortened PpTH-(3–41) and PpTHR-(3–41) analogues were undistinguishable from their full-size counterparts in activity against *Clavibacter* and *Rhizobium* but slightly less active against *Fusarium* and *Xanthomonas*. Again, the Arg^{32} substitution increased activity against all Gram-negative bacteria. Substantially shorter PpTH-(7–32) and PpTHR-(7–32) peptides were only slightly less active than the full-length parent structures against the pathogens tested, whereas the misfolded PpTH-(7–32)b was completely inactive against Gram-negative and fungal pathogens and marginally active against Gram-positive bacteria. The remaining peptides did not inhibit the growth of Gram-negative bacteria nor *F. oxysporum* and only PpTHR-(24–32) and PpTH-(7–19) were slightly active against *C. michiganensis*.

The correlation of antimicrobial activity with *in vivo* membrane permeabilization was investigated by monitoring the influx of SYTOX Green dye into *F. oxysporum* hyphae. This dye is able to penetrate cells with compromised membranes and fluoresces upon nucleic acid binding (33). Fungal hyphae incubated with 2-fold EC_{50} concentrations of the active peptides (PpTH, PpTH-(3–41), PpTH-(7–32), and their Arg^{32} analogues), showed a strong SYTOX Green fluorescence that was not detectable either in the absence of peptides (controls) or up to 20 μM concentration of the inactive peptides (PpTH-(24–32), PpTH-(7–19), PpTH-(15–28), and PpTH-(7–32)) (Fig. 4).

SPR Studies—The usefulness of SPR in studying the kinetics and thermodynamics of peptide binding to membranes is now well documented (34, 35). We have evaluated the binding activity of our most representative thionin analogues to anionic model membranes. To this end, DMPC/DMPG liposomes were captured onto a biosensor surface and association and dissociation of PpTH peptides was monitored. The corresponding sensorgrams clearly show that PpTH-(7–32) binds anionic membranes to a similar extent than full-length PpTH, whereas no interaction is detected at micromolar concentrations for (antimicrobially inactive) peptides PpTH-(24–32), PpTH-(7–19), and PpTH-(15–28) (Fig. 5). Both PpTH and PpTH-(7–32) bind very tightly to the liposomes and no regeneration of the immobilized bilayer is possible without resorting to non-ionic detergents. Sensorgrams were numerically fitted to a two-state reaction model to obtain kinetic and thermodynamic data (Table IV). Fittings to simpler models were unsuccessful.

TABLE IV
Association, dissociation, and affinity constants [a] of PpTH and PpTH-(7–32) for model membranes

	k_{on}^{1} (1/M·s)	k_{off}^{1} (1/s)	k_{on}^{2} (1/s)	k_{off}^{2} (1/s)	K (1/M)
PpTH	880	0.011	8.4×10^{-3}	7.33×10^{-4}	8.93×10^{5}
PpTH-(7–32)	1.02×10^{3}	1.17×10^{-3}	7.84×10^{-4}	1.27×10^{-3}	5.41×10^{5}

[a] Obtained by numerical integration of SPR data using a two-state reaction model. k_{on}^{1} and k_{off}^{1} are respectively the association and dissociation kinetic constants of the first step of the interaction; k_{on}^{2} and k_{off}^{2} refer similarly to the second step. K is the thermodynamic affinity constant (see Supplementary information).

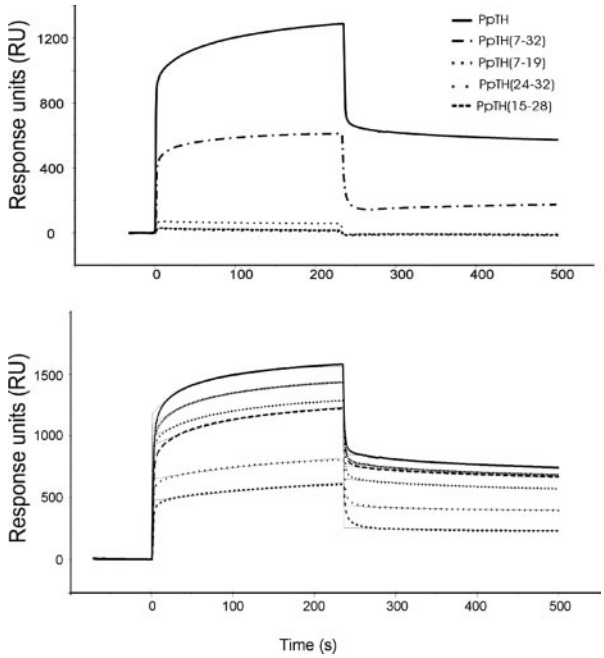

FIG. 5. **Thionin-membrane interaction studied by SPR.** *Top*: sensorgrams of PpTH, PpTH-(7–32), PpTH-(7–19), PpTH-(15–28), and PpTH-(24–32), all 40 μM, binding to model lipid bilayers. *Bottom*, sensorgrams of PpTH (in *bold*) binding to lipid bilayers at different concentrations, and fitted curves (*faint lines*) using the two-state reaction model.

DISCUSSION

Thionins are the first eukaryotic peptides for which antimicrobial activity against plant pathogens was demonstrated *in vitro* (18). Several other families of cystein-rich plant peptides have been characterized (22, 36) including plant defensins, lipid transfer proteins, hevein, and knottin-type peptides, and more recently snakins (37). Thionins alter the permeability and fluidity of microbial membranes and promote ion leakage through the formation of cation-selective channels (38). In an attempt to understand the structural basis for thionin activity and to define the minimal structural motif with relevant antimicrobial properties, we designed peptides mimicking several elements of *P. pubera* thionin (PpTH) secondary structure as well as shortened versions of PpTH to evaluate the role of its N- and C-terminal sections on antimicrobial activity. Synthetic approaches to multiple disulfide peptides (39, 40) were carefully adapted to obtain products with the desired native connectivity. For instance, in the oxidative procedure used for large PpTH analogues, the minimally denaturing conditions favor a folding process that drives formation of native-like disulfide connectivities. On the other hand, the substantially downsized two-disulfide thionins were not accessible by this procedure and required a chemoselective disulfide formation strategy.

Comparison of CD spectra, antimicrobial activities, and SYTOX Green influx was illustrative, in the sense that only peptides with well defined secondary structures, both in buffer and upon binding to model membranes, had biological activities akin to native thionin. Moreover, all fully active peptides had almost identical CD curves, with high helical contents and minimal temperature dependences. A possible interpretation for a membrane activity that does not require conformational change upon membrane binding has been advanced (7). As the rigid thionin structure makes it unlikely for the peptide to modify its polar/non-polar residue distribution through environment-induced conformational changes, a fact borne out by CD data, a possible explanation could be that thionins have environment-dependent association models. Thus, in aqueous solution self-association would cause hydrophobic residues to be buried in the core of the oligomer whereas, on reaching the membrane, the organizational pattern would be reversed and oligomers with hydrophobic residues exposed to the lipid membrane moieties would be formed, whereas hydrophilic regions would face the newly generated channel.

In marked contrast with the above, peptides PpTH-(7–32)b and PpTH-(15–28), which are random coil in water, can be induced into helical conformation in the presence of DMPG and display minimal antimicrobial activity. Cys pairing in the misfolded PpTH-(7–32)b does not force it into the antiparallel double helix active conformation (see below), but it is reasonable to assume that in the presence of lipid bilayers it might be able (as its disulfide bonds do not geometrically prevent it) to adopt a conformation capable of disrupting membranes and killing microorganisms, although at much higher concentrations, as seen here for *C. michiganensis*. The other analogue, PpTH-(15–28), is shown by SPR studies to interact very weakly with membranes and is only marginally active as an antibiotic. All this would suggest that, for this particular group of antimicrobial peptides, biological activity and conformational plasticity are not associated in a simple way. This agrees with previous studies (7, 41) showing poor correlation between peptide activity on either model membranes or intact bacteria, when the oligomerization state or volume of the peptide is crucial for the pore formation event (42).

Remarkably, the two shortened thionins, PpTH-(7–32) and PpTHR-(7–32), that we had designed to reproduce the antiparallel double α-helix core, retain the activity of full-length thionins against most tested organisms (*C. michiganensis*, *R. meliloti*, and *F. oxysporum*). The double helix folding, stabilized by the native-like Cys^{6}-Cys^{25} and Cys^{10}-Cys^{21} pairings, defines a characteristic amphipathic pattern and also contains residues shown to play a crucial role modulating thionin activity. Thus, iodination of Tyr^{13} of PpTH leads to a loss of toxicity (43, 44), suggesting that this residue is involved in the formation of transmembrane ion channels. Another sensitive position also present in our active, minimal versions of PpTH, is residue 32, the mutation of which (from Asp to Arg) significantly enhances activity against Gram-negative bacteria (17). The impact of this mutation is maintained along the PpTHR analogue series as long as the double helix folding pattern is preserved. Interestingly, even the tiny, 9-residue analogue PpTHR-(24–32), with only one of the two helices, is able to inhibit *C. michiganensis* growth at micromolar concentrations.

SPR studies also support that the double α-helix core is the structural motif responsible for the ability of thionins to bind to

microbial membranes and thus kill bacteria. Affinity constants of both full-length PpTH and PpTH-(7–32) for model membranes (Table IV) are of the same order of magnitude, whereas inactive peptides are completely devoid of interaction. The fact that a two-state reaction model is the best possible fit to the experimental data suggests that the mechanism of action of thionins involves an initial step of electrostatic binding to the outer face of the lipid bilayer followed by insertion into its hydrophobic core.

In conclusion, the present study shows that structure-guided deconstruction of a complex, highly knotted bioactive peptide such as PpTH can be used to reveal the main features responsible for its membrane-permeating, antibiotic activity. This information is not only useful in understanding the mechanism of action of this and similar families of antimicrobial peptides but can also be incorporated into the design of minimalist versions of such peptides with therapeutic potential.

Acknowledgments—We acknowledge technical help from G. López (ETISA, Madrid) and Dr. R. Gutiérrez-Gallego (Pompeu Fabra University) for helpful discussions on SPR.

REFERENCES

1. Boman, H. G. (2003) *J. Int. Med.* **254,** 197–215
2. Andreu, D., and Rivas, L. (1998) *Pept. Sci.* **47,** 415–433
3. Zasloff, M. (2002) *Nature* **415,** 389–395
4. Yeaman, M. R., and Yount, N. Y. (2003) *Pharmacol. Rev.* **55,** 27–55
5. Boman, H. G. (2000) *Immunol. Rev.* **173,** 5–16
6. Ganz, T., and Lehrer, R. I. (1999) *Mol. Med. Today* **5,** 292–297
7. Shai, Y. (2002) *Biopolymers* **66,** 236–248
8. Cohen, L. M. (1992) *Science* **257,** 1050–1054
9. Walsh, C. (2000) *Nature* **406,** 775–781
10. Cole, A. M., Hong, T., Nguyen, T., Zhao, C., Bristol, G., Zack, J. A., Waring, A. J., Yang, O. O., and Lehrer, R. I. (2002) *Proc. Natl. Acad. Sci. U. S. A.* **99,** 1813–1818
11. Liu, D., and DeGrado, W. F. (2001) *J. Am. Chem. Soc.* **123,** 7553–7559
12. Sitaram, N., Sai, K. P., Singh, S., Sankaran, K., and Nagaraj, R. (2002) *Antimicrob. Agents Chemother.* **46,** 2279–2283
13. Romestand, B., Molina, F., Richard, V., Roch, P., and Granier, C. (2003) *Eur. J. Biochem.* **270,** 2805–2813
14. Mangoni, M. L., Papo, N., Mignogna, G., Andreu, D., Shai, Y., Barra, D., and Simmaco, M. (2003) *Biochemistry* **42,** 14023–14035
15. Merrifield, R. B., Juvvadi, P., Andreu, D., Ubach, J., Boman, A., and Boman, H. G. (1995) *Proc. Natl. Acad. Sci. U. S. A.* **92,** 3449–3453
16. Andreu, D., Merrifield, R. B., Steiner, H., and Boman, H. G. (1983) *Proc. Natl. Acad. Sci. U. S. A.* **80,** 6475–6479
17. Vila-Perello, M., Sanchez-Vallet, A., Garcia-Olmedo, F., Molina, A., and Andreu, D. (2003) *FEBS Lett.* **536,** 215–219
18. Fernandez de Caleya, R., González-Pascual, B., García-Olmedo, F., and Carbonero, P. (1972) *Appl. Microbiol.* **23,** 998–1000
19. Carmona, M. J., Molina, A., Fernandez, J. A., Lopez-Fando, J. J., and Garcia-Olmedo, F. (1993) *Plant J.* **3,** 457–462
20. García-Olmedo, F., López-Fando, J. J., Castagnaro, A., Molina, A., Hernández-Lucas, C., and Carbonero, P. (1992) in *Genes Involved in Plant Defense* (Boller, T., and Meins, F., eds) pp. 283–302, Springer-Verlag, Wien
21. Osusky, M., Zhou, G., Osuska, L., Hancock, R. E., Kay, W. W., and Misra, S. (2000) *Nat. Biotechnol.* **18,** 1162–1166
22. García-Olmedo, F., Molina, A., Alamillo, J. M., and Rodríguez-Palenzuéla, P. (1998) *Pept. Sci.* **47,** 479–491
23. Caaveiro, J. M., Molina, A., González-Mañas, J. M., Rodríguez-Palenzuéla, P., García-Olmedo, F., and Goñi, F. M. (1997) *FEBS Lett.* **410,** 338–342
24. Lee, F. S., Chu, Z. T., and Warshel, A. (1993) *J. Comp. Chem.* **14,** 161
25. Guex, N., Diemand, A., and Peitsch, M. C. (1999) *Trends Biochem. Sci.* **24,** 364–367
26. Yount, N. Y., and Yeaman, M. R. (2004) *Proc. Natl. Acad. Sci. U. S. A.* **101,** 7363–7368
27. Fields, G. B., and Noble, R. L. (1990) *Int. J. Pept. Protein Res.* **35,** 161–214
28. Andreu, D., and Nicolás, E. (2000) in *Solid-phase Synthesis* (Kates, S. A., and Albericio, F., eds) pp. 365–375, Marcel Dekker, Inc., New York
29. Beringer, J. E. (1973) *J. Gen. Microbiol.* **84,** 188–198
30. Hackeng, T. M., Dawson, P. E., Kent, S. B., and Griffin, J. H. (1998) *Biopolymers* **46,** 53–63
31. Chen, Y.-H., and Yang, J. T. (1974) *Biochemistry* **13,** 3350–3359
32. Yang, J. T., Wu, C. S., and Martínez, H. M. (1986) *Methods Enzymol.* **130,** 208–269
33. Roth, B. L., Poot, M., Yue, S. T., and Millard, P. J. (1997) *Appl. Environ. Microbiol.* **63,** 2421–2431
34. Papo, N., and Shai, Y. (2003) *Biochemistry* **42,** 458–466
35. Mozsolits, H., and Aguilar, M. I. (2002) *Biopolymers* **66,** 3–18
36. Broekaert, W. F., Cammue, B. P., De Bolle, M. F., Thevissen, K., De Samblanx, G. W., and Osborn, R. W. (1997) *Crit. Rev. Plant Sci.* **16,** 297–323
37. Berrocal-Lobo, M., Segura, A., Moreno, M., Lopez, G., Garcia-Olmedo, F., and Molina, A. (2002) *Plant Physiol.* **128,** 951–961
38. Hughes, P., Dennis, E., Whitecross, M., Llewellyn, D., and Gage, P. (2000) *J. Biol. Chem.* **275,** 823–827
39. Andreu, D., Albericio, F., Solé, N. A., Munson, M. C., Ferrer, M., and Barany, G. (1994) in *Methods in Molecular Biology, Vol. 35: Peptide Synthesis Protocols* (Pennington, M. W., and Dunn, B. M., eds) pp. 91–169, Humana Press Inc., Totowa, NJ
40. Annis, I., Hargittai, B., and Barany, G. (1997) *Methods Enzymol.* **289,** 198–221
41. Avrahami, D., and Shai, Y. (2002) *Biochemistry* **41,** 2254–2263
42. Avrahami, D., Oren, Z., and Shai, Y. (2001) *Biochemistry* **40,** 12591–12603
43. Fracki, W. S., Li, D., Owen, N., Perry, C., Naisbitt, G. H., and Vernon, L. P. (1992) *Toxicon* **30,** 1427–1440
44. Wada, K., Ozaki, Y., Matsubara, H., and Yoshizumi, H. (1982) *J. Biochem.* (*Tokyo*) **91,** 257–263

Supplementary material to Vila-Perelló et al.:

"Structural dissection of a highly knotted peptide reveals minimal motif with antimicrobial activity"

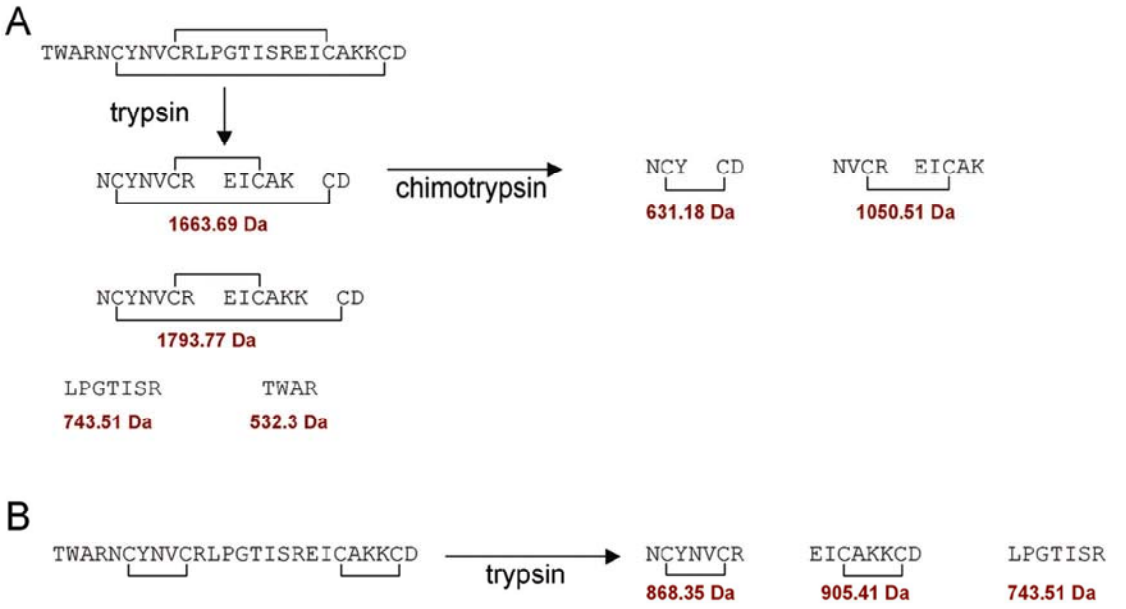

Figure S1: Determination of disulfide bridges of PpTH(7-32) and PpTH(7-32)b. Peptides (2 μg) were cleaved with trypsin in 50 mM Tris-HCl buffer, pH 8.0, for 2 h at 37 ºC. Reaction mixtures were analysed by HPLC and MALDI-TOF MS. (A) For PpTH(7-32), the main product with MW 1663.7 Da was isolated and subsequently incubated with chymotrypsin in 50 mM Tris-HCl, 10 mM $CaCl_2$, 1 h at 37 ºC, to give two disulfide-linked fragments (MWs 631.2 and 1050.5 Da) that unequivocally revealed the disulfide bridge pattern. (B) For PpTH(7-32)b, analysis of the tryptic digest by MALDI-TOF MS allowed straightforward assignment of Cys pairings.

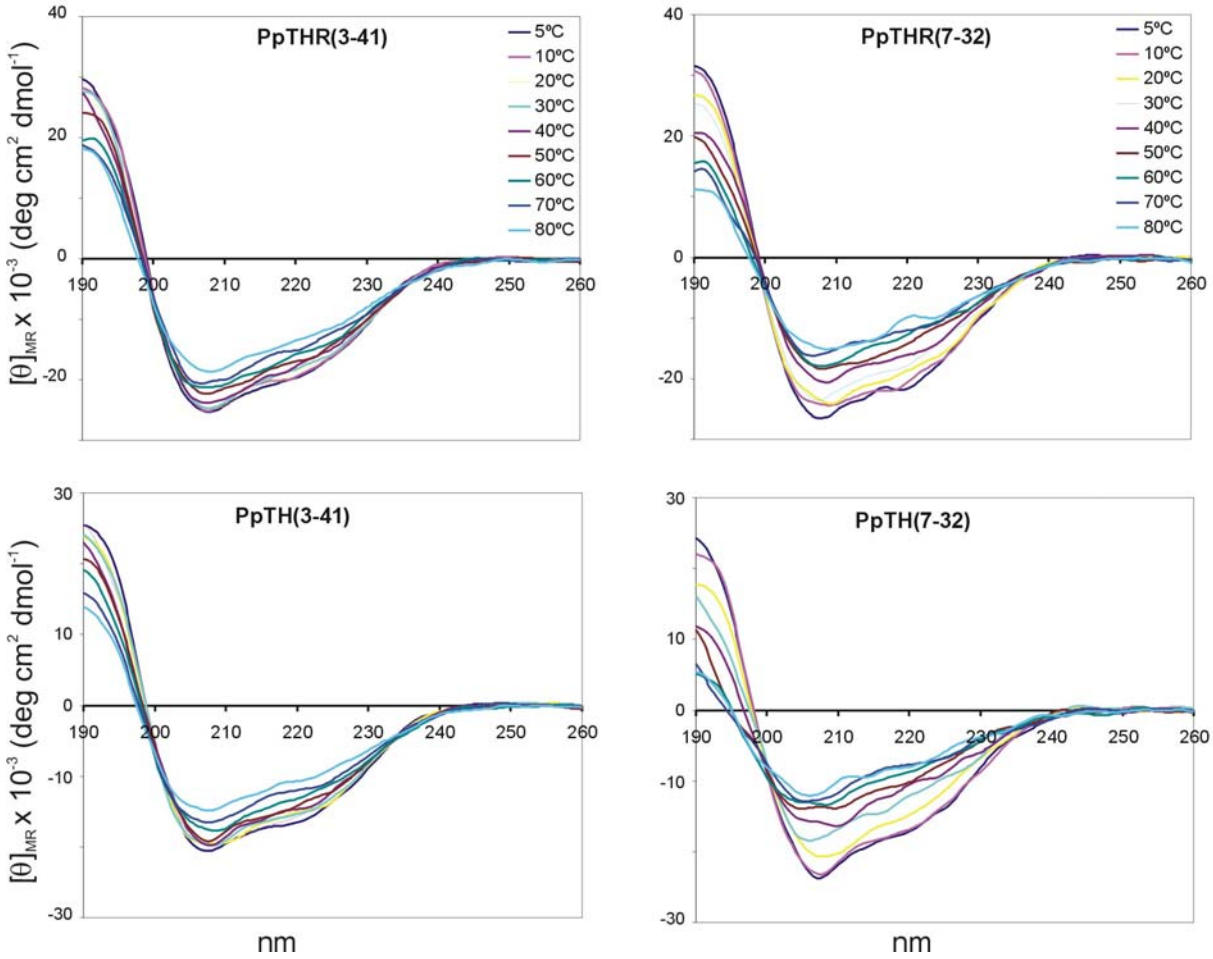

Figure S2: Effect of temperature on secondary structure of PpTH peptides. CD curves were recorded at 15 μM peptide concentration in 25 mM phosphate buffer, pH 6.0, at nine temperatures within the 5-80 ºC range, using a 20 ºC/h ramp. For each spectra two scans from 190 to 260 nm were accumulated at 100 nm/min with 0.5 nm resolution, 2 s response and 1.0 nm bandwidth.

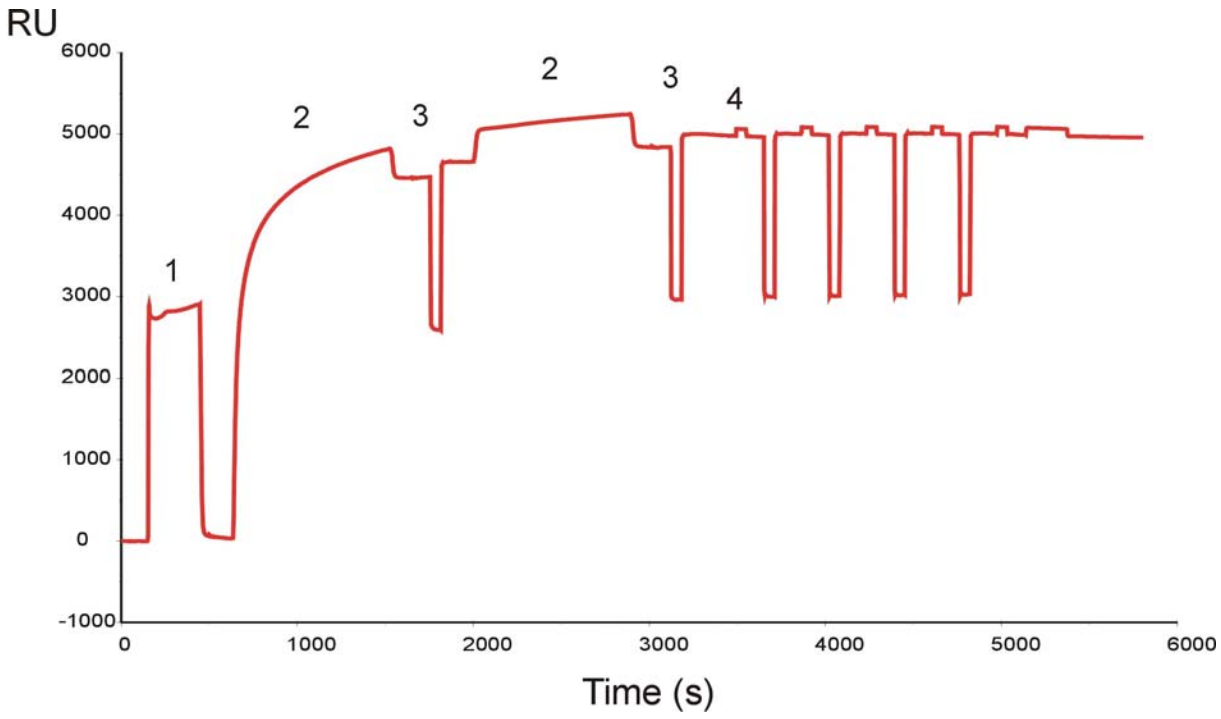

Figure S3: Sensorgram of the immobilization of DMPC/DMPG liposomes on a L1 chip. 1) Injection of 25 μl of 40 mM n-octyl-β-glucopyranoside at 5 μl/min flow rate was performed to clean the chip surface. 2) Liposomes were applied to the sensor surface at a 2 μl/min flow rate. After each liposome injection, a 50 μl pulse of 10 mM NaOH at 50 μl/min (3) was applied to remove multilamellar structures. Finally, the active surface was stabilized by repeated injections of 10 mM NaOH and PBS buffer (4) until a stable baseline was obtained.

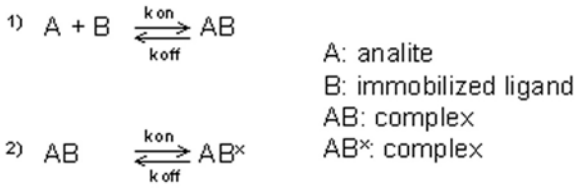

Total response:

AB + ABx

B[0] = Rmax

dB/dt = - (kon1*A*B - koff1*AB)

AB[0] = 0

dAB/dt = (kon1*A*B - koff1*AB) - (kon2*AB - koff2*ABx)

ABx[0] = 0

dABx/dt = (kon2*AB - koff2*ABx)

K = (kon1/Koff1) x (kon2/koff2)

Figure S4: The two state reaction model. In the first step, peptide analyte (A) binds to liposomes (B) to yield AB which is transformed to AB^X in the second step and cannot dissociate to A + B. The first process may correspond to electrostatic interaction between the peptide and the model membrane and the second one to partial insertion of bound peptide into the membrane.

Structural Dissection of a Highly Knotted Peptide Reveals Minimal Motif with Antimicrobial Activity

Miquel Vila-Perelló, Andrea Sánchez-Vallet, Francisco García-Olmedo, Antonio Molina and David Andreu

J. Biol. Chem. 2005, 280:1661-1668.
doi: 10.1074/jbc.M410577200 originally published online October 19, 2004
